

Quantifying the Absorption Onset in the Quantum Efficiency of Emerging Photovoltaic Devices

Osbel Almora,* Carlos I. Cabrera, Jose Garcia-Cerrillo, Thomas Kirchartz, Uwe Rau, and Christoph J. Brabec*

The external quantum efficiency (EQE), also known as incident-photon-to-collected-electron spectra are typically used to access the energy dependent photocurrent losses for photovoltaic devices. The integral over the EQE spectrum results in the theoretical short-circuit current under a given incident illumination spectrum. Additionally, one can also estimate the photovoltaic bandgap energy (E_g) from the inflection point in the absorption threshold region. The latter has recently been implemented in the “Emerging PV reports,” where the highest power conversion efficiencies are listed for different application categories, as a function of E_g . Furthermore, the device performance is put into perspective thereby relating it to the corresponding theoretical limit in the Shockley–Queisser (SQ) model. Here, the evaluation of the EQE spectrum through the sigmoid function is discussed and proven to effectively report the E_g value and the sigmoid wavelength range λ_s , which quantifies the steepness of the absorption onset. It is also shown how EQE spectra with large λ_s indicate significant photovoltage losses and present the corresponding implications on the photocurrent SQ model. Similarly, the difference between the photovoltaic and optical bandgap is analyzed in terms of λ_s .

primary characterization of photovoltaic (PV) devices,^[1,2] along with the current density-voltage ($J - V$) characteristic. Most typically, the $J - V$ curve at a given temperature (T) and under a given steady-state illumination power density (P_{in}) provides the performance parameters of the cell: power conversion efficiency (PCE), open-circuit voltage (V_{oc}), short-circuit current density (J_{sc}) and fill factor (FF). On the other hand, the EQE allows to discern how the charge collection behaves as a function of the incident photon energy (E) and one can estimate both the PV device bandgap energy (E_g , also labeled $E_{g,pv}$) and the theoretical J_{sc} under a given illumination, for example, 1 sun = 100 mW·cm⁻² standard AM1.5G spectrum ($\Gamma_{AM1.5G}$). In single-junction-like solar cells, this set of device measurement parameters (T , P_{in} , E_g) allows one to estimate the detailed-balance limit for each performance parameter (PCE, V_{oc} , J_{sc} , FF), also known as the Shockley–Queisser (SQ) limit.^[3–5]

1. Introduction


The external quantum efficiency (EQE) of a solar cell, sometimes referred to as the incident photon-to-collected-electron conversion efficiency, is one of the most frequently used techniques for the

Experimentally, the EQE is measured by obtaining the current density response (J_λ) per unit incident illumination power density (P_λ), as a function of the incident photon energy or wavelength (λ). In addition, J_λ can change with the voltage bias (V) applied to the device, the incident direct-current (DC) mode

Dr. O. Almora
Institute of Advanced Materials
Universitat Jaume I
Castellón de la Plana S12006, Spain
E-mail: osbel.almora@fau.de

Dr. O. Almora, Prof. C. J. Brabec
Erlangen Graduate School in Advanced Optical Technologies
Friedrich-Alexander-Universität Erlangen-Nürnberg
91052 Erlangen, Germany
E-mail: christoph.brabec@fau.de

Dr. C. I. Cabrera
Consejo Zacatecano de Ciencia
Tecnología e Innovación
Zacatecas 98090, Mexico

 The ORCID identification number(s) for the author(s) of this article can be found under <https://doi.org/10.1002/aenm.202100022>.

© 2021 The Authors. Advanced Energy Materials published by Wiley-VCH GmbH. This is an open access article under the terms of the Creative Commons Attribution-NonCommercial License, which permits use, distribution and reproduction in any medium, provided the original work is properly cited and is not used for commercial purposes.

DOI: 10.1002/aenm.202100022

J. Garcia-Cerrillo, Prof. C. J. Brabec
Institute of Materials for Electronics and Energy Technology
Friedrich-Alexander-Universität Erlangen-Nürnberg
91058 Erlangen, Germany

Prof. T. Kirchartz, Prof. U. Rau
IEK5-Photovoltaics
Forschungszentrum Jülich
52425 Jülich, Germany

Prof. T. Kirchartz
Faculty of Engineering and CENIDE
University of Duisburg-Essen
47057 Duisburg, Germany

Prof. C. J. Brabec
Forschungszentrum Jülich GmbH
Helmholtz-Institut Erlangen-Nürnberg for Renewable Energy (HI ERN)
91058 Erlangen, Germany

Prof. C. J. Brabec
Zernike Institute for Advanced Materials
University of Groningen
Groningen 9712, The Netherlands

background illumination power density (P_{in}) and the angular frequency (ω) of the alternating-current (AC) mode chopping/modulation corresponding to the monochromatic light. Accordingly, the corresponding spectrum results as,

$$EQE(\lambda, P_{in}, V, \omega) = \frac{hc}{\lambda q} \frac{J_{\lambda}(\lambda, P_{in}, V, \omega)}{P_{\lambda}} \quad (1)$$

where q is the elementary charge, h is the Planck's constant, and c is the speed of light. Note that, although the spectral responsivity $S(\lambda) = J_{\lambda}/P_{\lambda}$ can be obtained in steady state ($\omega \rightarrow 0$), for practical reasons the AC mode is the preferred method, typically using choppers with lock-in amplifiers^[1] or potentiostats for intensity modulated photocurrent spectroscopy (IMPS).^[6,7]

At short-circuit ($V = 0$), and arguably preferable under simulated background 1 sun illumination intensity, one can estimate the theoretical photocurrent under $\Gamma_{AM1.5G}$ (in units of $W \cdot m^{-2} \cdot nm^{-1}$) according to the integral,

$$J_{sc} = \frac{q}{hc} \int EQE(\lambda) \cdot \lambda \cdot \Gamma_{AM1.5G}(\lambda) d\lambda \quad (2)$$

The agreement between J_{sc} from the $J - V$ curve and that after Equation (2) from the EQE spectrum can be understood as an assessment on how well both measurement conditions were equivalent and how much the simulated light spectrum approached $\Gamma_{AM1.5G}$ for the $J - V$ curve.

However, care must be taken with the measurement and subsequent analyses of the EQE spectra. For instance, Saliba & Etgar^[8] recently surveyed on several factors producing significant mismatch between photocurrents calculated from EQE and $J - V$ curves in perovskite solar cells (PSCs). Some of these issues are not only present in PSCs, but are found among organic PV cells (OPVs) and dye sensitized solar cells (DSSCs), which report decreased EQE spectra as the DC illumination intensity increases (see Figure 1a).^[2,9] Similarly, the AC modulation/chopping frequency has been reported to modify the spectra in PSCs^[1] and DSSCs^[10] (see Figure 1b), and in both cases^[11,12] the presence of $J - V$ hysteresis (see Figure 1c) due to ionic conductivity and/or performance instability can also be the cause of artifacts. Although these effects are more characteristic of low efficiency devices, another minor influence can be the poor precision in the EQE measurement and the $\Gamma_{AM1.5G}$ spectrum interpolation: wavelength steps ≥ 10 nm are not encouraged (see Figure S1, Supporting Information). Interestingly, Dunbar et al.^[13] have proposed a re-normalization method for identifying possible issues in the EQE measurement when the integrated photocurrent exceeds 95% of the ideal value provided by the SQ model.

Nevertheless, the use of EQE spectra is encouraged in the recent "Emerging PV reports"^[14] for validating performance parameters, especially for estimating the E_g value as a reference for putting each report in perspective to the SQ model at the appropriate E_g . Since the SQ-model idealizes the EQE to a step function with E_g as the threshold energy, a proper definition of a reference bandgap for real world (non-step function) EQEs is crucial, as discussed in the literature.^[5,15,16] In the "Emerging PV reports,"^[14] the E_g is taken as the inflection point of the EQE spectra in the absorption threshold region, by fitting to a sigmoid function. This procedure represents a parameteri-

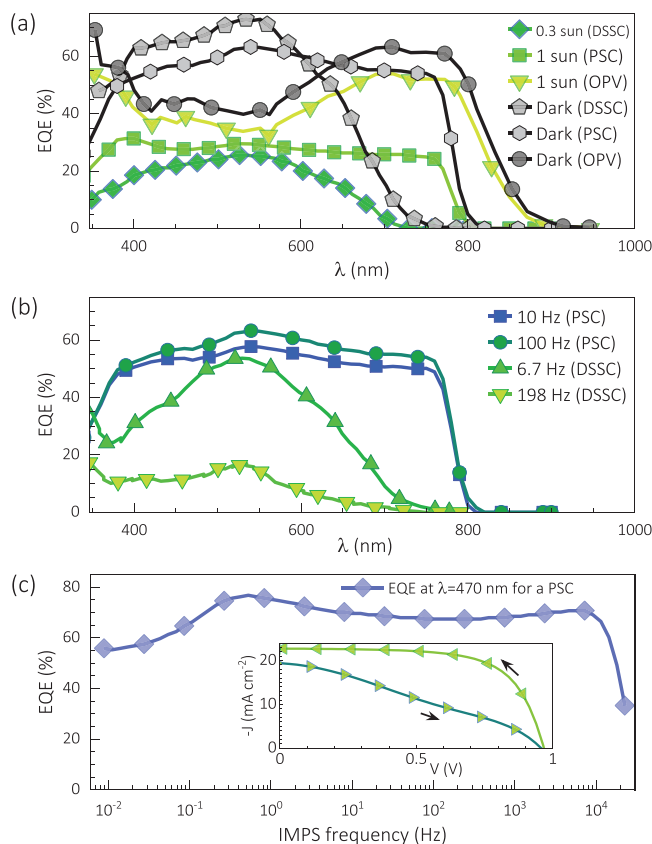


Figure 1. Typical factors affecting the EQE measurement and subsequent estimation of J_{sc} and/or E_g : a) background dark/illumination, and frequency modulation with b) chopper and d) IMPS. In (a), the examples of an OPV (adapted with permission.^[2] Copyright 2012, Elsevier) and a DSSC (adapted with permission.^[9] Copyright 2012, Elsevier) are displayed. In (b), the data belongs to a PSC (see Section S1, Supporting Information) and a DSSC (adapted with permission.^[10] Copyright 2012, IOP Publishing, Ltd.). In (c), the data correspond to PSCs: the inset $J - V$ curves are adapted with permission.^[33] Copyright 2019, Elsevier, and the IMPS spectrum is adapted with permission.^[1] Copyright 2018, American Chemical Society.

zation of the definition of PV bandgap energy ($E_{g,pv}$) given by Rau et al.,^[15] although one can find several alternative methods for extracting E_g from the EQE.^[17]

The $E_{g,pv}$ does not necessarily match the optical bandgap energy $E_{g,op}$, typically obtained from Tauc plots derived from absorption measurements.^[18] The bandgap energy $E_{g,op}$ determined by absorption measurements represents an internal property of the absorber *material*. In contrast, the SQ-model uses the bandgap energy as an external threshold value to describe the solar cell *device*.^[16] The theoretical basis of $E_{g,op}$ has also been questioned since it assumes free carrier, rather than excitonic, absorption edges, reporting values reduced by the excitonic binding energy and a thermal broadening parameter.^[19,20] On the other hand, the $E_{g,pv}$ from EQE spectra characterizes the occupied density of states, as defined in the full *device* rather than in the individual absorber *material*, and includes all the excitonic and/or thermal broadening contributions, as well as the geometrical features of the device, for example, the thickness.

Interestingly, the first version of "Emerging PV reports"^[14] presented several J_{sc} values (from the $J - V$ curves) exceeding

their SQ limit for PSCs^[21–23] and DSSCs.^[24,25] Note that in all of these cases the J_{sc} from the integrated EQE spectrum was below the SQ limit, indicating the influence of effects such as hysteresis, over-illumination or effective area underestimation. Alternatively, it may have happened that the EQE spectra did not correspond to the best device whose $J - V$ curve parameters were reported. Moreover, these reports also questioned whether the EQE is the most appropriate method for estimating E_g and how to deal with different shapes of the EQE spectra regarding the SQ model. For instance, EQE spectra with low slope in the absorption threshold are frequently found among amorphous silicon solar cells (a-Si:H),^[26,27] DSSCs,^[9,24,28] OPVs,^[26] PSCs,^[29,30] quantum dot sensitized solar cells,^[31] and Sb₂Se₃-based cells.^[32] In addition, the difference between PV and optical bandgap energy and its interpretation persists as a subject of discussion.

In the present paper, the measurement and analysis of the EQE spectrum for evaluation of the E_g , and the theoretical efficiency limits in emerging PV technologies are discussed. The sigmoid parameterization for evaluating the PV E_g in the “Emerging PV reports”^[14] is further introduced and discussed, focusing on the useful quantifying parameter λ_s herein called sigmoid wavelength, or sloping wavelength range of the absorption threshold. The matter on how the SQ limit is influenced by λ_s is addressed, in relation with typical non-idealities in the EQE spectra. Moreover, the difference between PV and optical bandgap is also analyzed in terms of λ_s and the corresponding energy range E_s .

1.1. The PV Bandgap through the Sigmoid Function

In classical semiconductor physics, the bandgap energy E_g is the difference between the energy levels for the top and bottom of the valence and conduction bands, respectively. That range of energy values is theoretically forbidden to electrons. Thus, an electron in the top of the valence band would need an energy $E \geq E_g$ to reach the conduction band in order to contribute to electronic current. Assuming an incoming energy to the system as photon flux, it would be expected that only those photons with $E \geq E_g$ could generate charge carriers to be extracted as photocurrent when the absorber material is part of a selective structure forming a PV device. At this point, it is clear that the evaluation of E_g could be performed by an optical approach to the absorbance (A) spectrum, for example, measuring transmittance (T) and reflectance (R) or in an optoelectronic way through the EQE spectrum. In the SQ model of an ideal solar cell, both A and EQE spectra should approach unity for $E \geq E_g$ and zero elsewhere.

In practice, the device structure and fabrication methods may modify the optoelectronic properties of the device, producing a mismatch $\Delta E_g = E_{g,pv} - E_{g,op}$ between the optical value and the so-called PV bandgap. Note that the presence of ΔE_g indicates a different absorption offset between the EQE and the internal quantum efficiency $IQE = EQE/(1 - T - R)$.

“Pure” step function EQE spectra are not found in the experiment. Instead, smoother absorption thresholds occur whose shapes resemble more a sigmoid function. Accordingly, the E_g value can be obtained from the inflection point of the EQE

spectrum by locating the maximum in the spectra derivative $\partial EQE/\partial E$ (or $\partial EQE/\partial \lambda$). Alternatively, one can parameterize the absorption threshold as,

$$EQE(\lambda) = \frac{A_m}{1 + \exp[\kappa(\lambda - \lambda_g)/\lambda_s]} \quad (3)$$

where $\kappa = \ln[7 + 4\sqrt{3}] \cong 2.63$ is a numeric factor that results from calculating the roots of the second derivative (see **Figure 2a**). The PV device bandgap relates to the corresponding wavelength as,

$$E_g = \frac{hc}{\lambda_g} \quad (4)$$

and A_m and λ_s are fitting parameters related to the maximum EQE just after the step and the slope during the step (see **Figure 2a**), herein also called the sigmoid maximum and sigmoid wavelength range, respectively. While the position of λ_g corresponds to the inflection point of $EQE(\lambda)$, that is, the maximum of the Gaussian-like first derivative $\partial EQE/\partial \lambda$, the λ_s value is the distance between the maximum and minimum of the second derivative $\partial^2 EQE/\partial \lambda^2$ (see **Figure 2a**). Importantly, note that the bandgap from definitions (3) and (4) are not necessarily matching the optical bandgap from typical linear fits

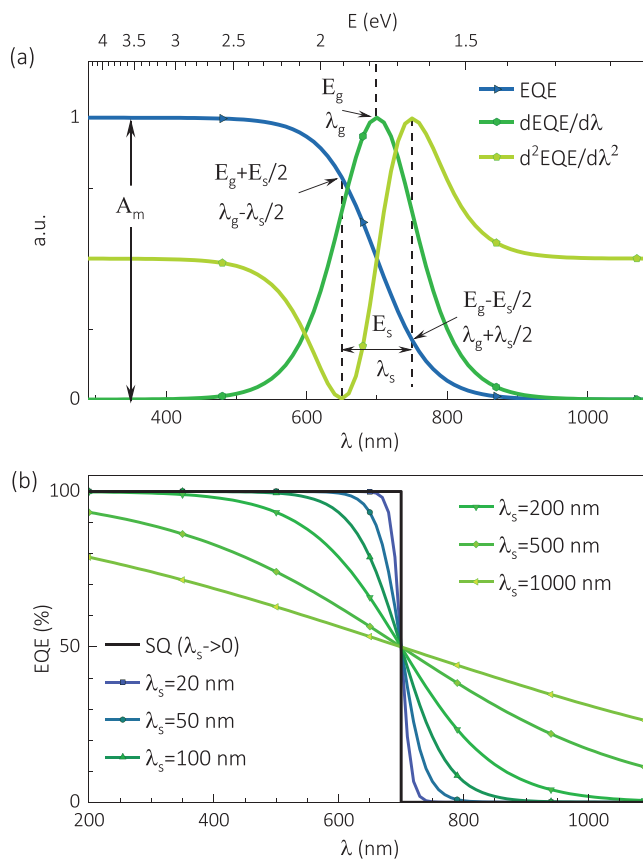


Figure 2. Sigmoid parameterization of EQE spectra: a) schematics of physical meaning of sigmoid fitting parameters and b) different EQE spectra for several values of the sigmoid sloping wavelength. The derivative plots in (a) are normalized.

for Tauc plots of the absorption spectrum (see Section 3),^[18,34] or other alternative methods.

In experimental spectra, one would expect the inflection point of the EQE spectrum to lie somewhere between the 20% and the 80% (ideally at 50%) of the maximum value. However, for $\lambda_s > 200$ nm, the maximum A_m is hardly found within the typical wavelength measurement ranges, as illustrated in Figure 2b, which hinders the evaluation of λ_g .

The sigmoid is a relatively simple analytical function that resembles the Fermi–Dirac distribution and avoids the numerical complications of similar metrics, such as the error function.^[35] The sigmoid parameterization can be advantageous for automatized EQE data processing because λ_g and λ_s are taken directly from the EQE spectrum. In contrast, alternative methods calculate first the derivative $\partial EQE/\partial E$ and subsequently locate their maximum, or apply a fitting to the derivative (e.g., see Rau and Werner).^[36]

At this point, it is already suggested that the E_g value results straightly from the corresponding λ_g in the sigmoid parameterization of Equation (3) for $\lambda_s < 100$ nm when the EQE spectrum is presented as a function of the wavelength. In this situation, the PV bandgap energy is effectively defined as the inflection point of the EQE spectrum in the region of the absorption threshold, analogously to the conclusions by Rau et al.^[15] and the analyses by Green & Ho-Baillie^[19] and Krückemeier et al.^[16]

1.2. Some Typical Non-Idealities

The use of Equation (3) can be “easy,” as in the case of Figure 3a, where there are no significant deviations from the

sigmoid behavior and small values for λ_s are found. This happens when the absorption threshold region is narrow enough, thus the sigmoid parameterization approaches well the SQ assumption. Then, the integrated J_{sc} from the experiment and the sigmoid parameterization are lower than that for the SQ model (see Figure 3a and Figure S2a, Supporting Information). This can be called an “ideal” EQE spectrum.

Differently, the sigmoid approach finds some issues when the shape of the EQE spectrum is like those in Figure 3b,c. For instance, although the absorption threshold is narrow (small λ_s) in Figure 3b, the presence of extra sensitizers increases charge collection well above λ_g (below E_g), fostering the integrated photocurrent (see Figure S2b, Supporting Information). In this case, the “single junction” assumption in the SQ model would arguably be unsatisfied, and one would be tempted to consider a lower E_g (higher λ_g) value corresponding to the sensitizer compound. Taking a lower E_g (higher λ_g) value would, in general, misread the real performance of the device, and besides, particular care should be taken with the sensitivity of sub-bandgap regions in the EQE spectra due to several sources of acoustic and electrical noise, as well as deep trap states with a spectral shape affected by micro-cavity interference.^[37] Moreover, the example of Figure 3b would be called a “non-ideal” EQE spectrum in terms of the SQ model.

Widespread absorption threshold spectra (large λ_s) may be very symmetric, such as in Figure 3c, but the integrated photocurrent for the experiment and the sigmoid fitting could be above that for the SQ limit (see Figure S2c, Supporting Information). Thus, one would also say that this is a “non-ideal” EQE spectrum. In this case, the irregular distribution of the photon flux makes the region of the EQE spectrum above λ_g

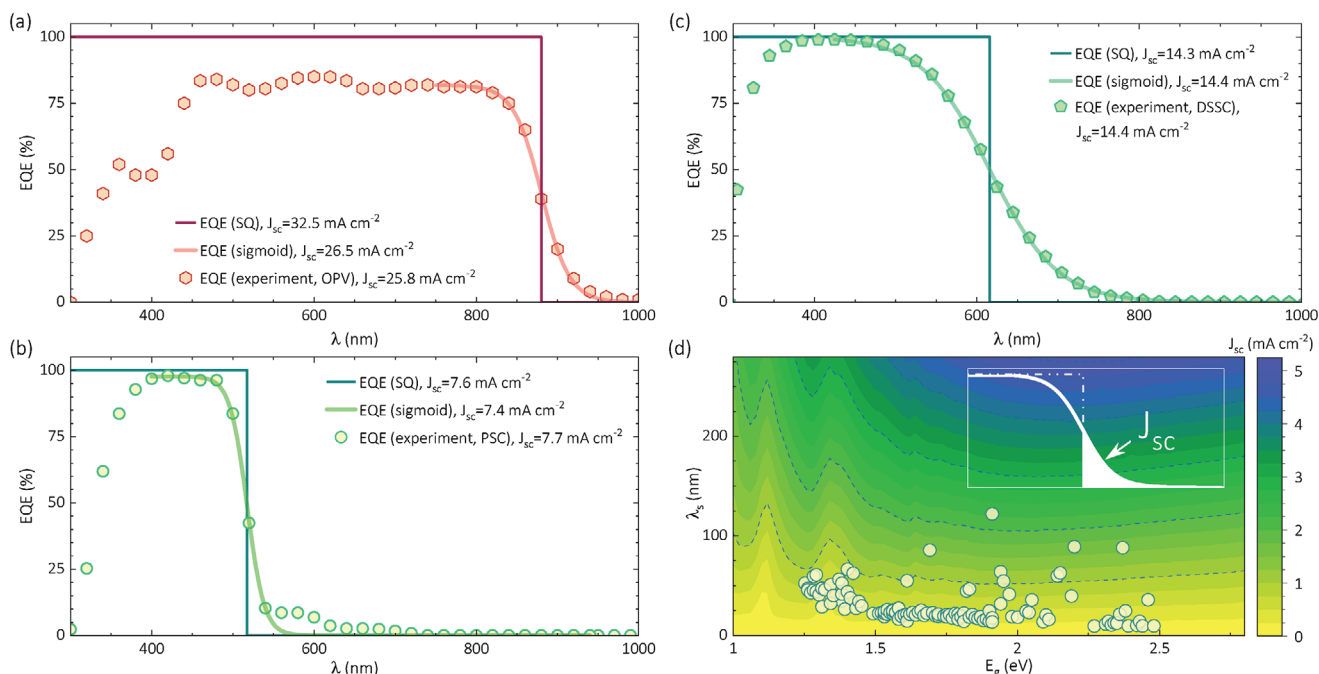


Figure 3. Illustrative EQE spectra for experimentally a) “ideal” and b,c) “non-ideal” cases, and d) integrated photocurrent for the sub-bandgap range (integral (2) from λ_g to ∞) assuming sigmoid EQE spectra. Data in (a) belongs to an OPV (adapted with permission.^[38] Copyright 2019, Wiley); the spectra in (b) and (c) resemble those reported for a PSC^[21] and a DSSC,^[24] respectively; and the data (circles) in (d) correspond to PSCs in the “Emerging PV reports.”^[14] The specified photocurrent integrals in (a–c) are shown in Figure S2, Supporting Information.

(below E_g) to contribute more to the integral. The contour plot of Figure 3d shows the integration of J_{sc} following Equation (2) between λ_g and infinity for λ_s values up to 280 nm. One can see that for $E_g > 1.5$ eV we may have extra contributions to the short circuit current > 2 mA \cdot cm $^{-2}$ for $\lambda_s > 100$ nm.

For further understanding large λ_s values in EQE spectra, one can approach the photocurrent factor in the definition (2), assuming steady state in an absorber of thickness L with homogeneous generation rate G for the appropriate wavelength range, around λ_g , resulting

$$J_\lambda \approx qL(G(\lambda) - R(\lambda)) \quad (5)$$

where G is proportional to the absorption coefficient $\alpha(\lambda) = hcG(\lambda)/\lambda P_\lambda$, for example, considering a weak absorption in a thin film, and R is the recombination rate. Subsequently, one can rewrite Equation (1) as,

$$\text{EQE}(\lambda) = L \left(\alpha(\lambda) - \frac{hc}{\lambda} \frac{R}{P_\lambda} \right) \quad (6)$$

The first term in Equation (6) can also be obtained by a Taylor expansion of the Lambert–Beer model.^[16] The shape of the EQE spectrum may depend on both $\alpha(\lambda)$ and R contributions. Neglecting energy dependency in R , one can assume in the vicinity of λ_g that $\alpha \propto \exp[-2.63 \lambda/\lambda_s]$. This behavior in the energy representation resembles that of $\alpha \propto \exp[E/E_U]$ characterized by the Urbach energy E_U .^[39,40] Small values of E_U are typically associated with a high structural quality of the absorber material, convenient optoelectronic properties, such as a high carrier mobility, and minimal photovoltage losses.^[41–44] With the proper operations, it can be demonstrated that $\lambda_s \propto E_U$ in the range $E_U \ll E < E_g$, which is intuitive since both parameters affect similarly the logarithmic slope. For instance, the recent work by Vandewal et al.^[45] estimated the voltage losses related to broader EQE tails due to charge transfer states in the low-energy sub-gap regime of OPVs. Likewise, λ_s should be proportional to the standard deviation of the error function used in the parameterization of Hood et al.^[35] for evaluating disorder in organic semiconductors.

It can also be found that devices with different architectures and/or doping profiles present different absorption threshold in the EQE spectra due to $R(\lambda)$ features. This is typically evidenced via the IQE spectrum, whose change depending on the wavelength range has been reported in several technologies.^[46–48] The most common effect of energy dependent recombination rate relates to the difference in charge carrier density, due to inhomogeneous G . This is typical in thick devices, such as silicon solar cells, where the diffusion limited transport favors the surface recombination toward the contacts for the larger or shorter absorbed photon energies.^[49–51]

The radiative recombination coefficient $\kappa_{\text{rad}} \propto n_{\text{abs}}^2(\lambda) A(\lambda) \Phi_{\text{BB}}(\lambda)$ could also be of significant influence,^[52] mainly through the energy dependency of the refractive index n_{abs} , since the black body photon flux Φ_{BB} peaks at $\lambda > 8$ μm for typical cell operation temperatures. More exotically, one may find a trap recombination coefficient $\kappa_t \propto \left(\frac{hc}{\lambda} - E_g \right)^{-1/2}$ favoring Shockley–Read–Hall recombination for charge carriers

generated by photons with energy close to E_g , given small electron-phonon and electron-electron scattering rates for long thermalization times.^[53] For instance, for polymer-fullerene solar cells,^[54] it has been found that photo-generated carriers can be extracted from the operating device before reaching thermal equilibrium. Furthermore, note that interference can be a significant energy-dependent effect, as pointed out by Armin et al.^[55] in their study on bulk-heterojunction solar cells with a parameterization based on the non-adiabatic Marcus theory for charge transfer states in the sub-bandgap region.

Summing up, “good devices” with small- E_U -absorbers and low non-radiative recombination are expected to present small λ_s values in the EQE. The non-idealities in the EQE spectra (large λ_s or asymmetries) can be tackled in detail, attending to their particular nature, as proposed in Section S2, Supporting Information. Nevertheless, from Figure 3d one can easily get an estimation on how increasing λ_s values imply large integrated photocurrent for photon energies below E_g (wavelengths above λ_g). This, of course, leads to the discussion on how the photovoltage is affected by large λ_s values and whether the theoretical performance limit is modified. Would photocurrents above the SQ limit mean efficiencies larger than those considered after the detailed balance principle?

2. On the SQ Model

The sigmoid parameterization is one of the easiest analytical approximations for the step function EQE spectrum used in the SQ model as $\lambda_s \rightarrow 0$. Thus, at this point one would want to know what range of λ_s makes a good approximation of Equation (3) for the SQ assumption. Accordingly, the SQ limit is calculated by numerically locating the maximum power point (MPP) for ideal $J - V$ curves with the form,

$$J = J_0^{\text{rad}} \left(\exp \left[\frac{qV}{k_B T} \right] - 1 \right) - J_{sc} \quad (7)$$

where k_B is the Boltzmann constant, J_{sc} is the photocurrent matching the integral of Equation (3) for different λ_s values, and the radiative saturation current follows the detailed balance principle as^[3,4,56]

$$J_0^{\text{rad}} = f_e 2\pi q c \int_0^{+\infty} \text{EQE}(\lambda) \left(\exp \left[\frac{hc}{\lambda k_B T} \right] - 1 \right)^{-1} \frac{d\lambda}{\lambda^4} \quad (8)$$

where $f_e = 2$ accounts for the emission from both the front and rear contacts of the cell, or $f_e = 1$ for emission only via the front side. Note that the ideal assumption entering $f_e = 2$ into Equation (8) implies identical quantum efficiencies for front absorption and both front and rear emission, that is, $\text{EQE}_{\text{abs,front}} = \text{EQE}_{\text{em,front}} = \text{EQE}_{\text{em,back}}$. It is further assumed that there is no angular dependence of the EQE and hence no angular dependence of the luminescence emission. In the real devices, the EQE spectra for the PV absorption and luminescence emission have angular dependence and may be significantly different regarding the front and rear sides of the cell.

With this, one can set $J = 0$ in Equation (7) for deducing the ideal radiative limit for the open-circuit voltage as

$$V_{oc}^{rad} = \frac{k_B T}{q} \ln \left[\frac{J_{sc}}{J_0^{rad}} + 1 \right] \quad (9)$$

which is proportional to the logarithm of the ratio between generation (J_{sc}) and emission (J_0^{rad}).

The substitution of the sigmoid Equation (3) into Equations (2) and (8) and then into (9), allows us to determine the complete $J - V$ characteristics and, hence all PV performance parameters (J_{sc} , V_{oc} , FF, PCE) as a function of λ_g and λ_s under the assumption that the only allowed recombination mechanism is radiative recombination followed by photon emission. As opposed to the original SQ approach (assuming a step-function like EQE), this radiative limit is based on a “real-world EQE” of a “real-world solar cell” but otherwise under the idealizing assumption of radiative recombination only.

The simulated radiative limit was calculated for different values of λ_s , from 20 to 1000 nm (see Figure 4). As already noted in the previous section, Figure 4a shows that EQE spectra with $\lambda_s \geq 100$ nm result in integrated photocurrents above those of the SQ model for $E_g > 1.8$ eV. However, as λ_s approaches and exceeds 100 nm, the emissive losses are also significantly affected, increasing J_0^{rad} , and thus reducing the V_{oc} , which is illustrated in Figure 4b. The stronger photovoltage losses are respectively shown in Figure 4b,c to lower the limiting values for V_{oc} and PCE as λ_s increases. In other words, although large λ_s values do produce J_{sc} above the values of the traditional SQ case, the broadening of the absorption threshold in the EQE spectra strongly reduces the maximum achievable V_{oc} and, consequently, efficiency with respect to the values provided by the SQ model to those in the radiative limit.

The substantial need for consistency in terms of detailed balance and reciprocity can be demonstrated by neglecting the emission contribution below E_g (above E_g), that is, take the λ_s effect only for the photocurrent integration in Equation (3) but using the traditional SQ step function ($\lambda_s \rightarrow 0$) for the saturation current in Equation (8). Since such assumption clearly violates reciprocity (e.g., Equation (8)), no significant reduction in the V_{oc}^{rad} produces unrealistically large values for FF and PCE above the ideal SQ limit for $\lambda_s \geq 100$ nm (see Figure S4, Supporting Information).

Importantly, photocurrents above the ideal SQ limit in Figure 4a are a correction to the SQ model resulting from the broadening λ_s of the absorption threshold. Note that even in the experiments there are some reports of photocurrent values above the SQ value, but none beyond the efficiency or photovoltage SQ values, as recently surveyed in the “Emerging PV reports.”^[14] This finding demonstrates how careful the term SQ limit should be handled and that it is more advisable to use the term SQ model. This model predicts PV parameters as a function of bandgap energy under the strict assumption of a step-like EQE, and note that it is only a valid limit in terms of current at the optimum bandgap.^[57] For bandgap energies above the optimum, adding some EQE below the

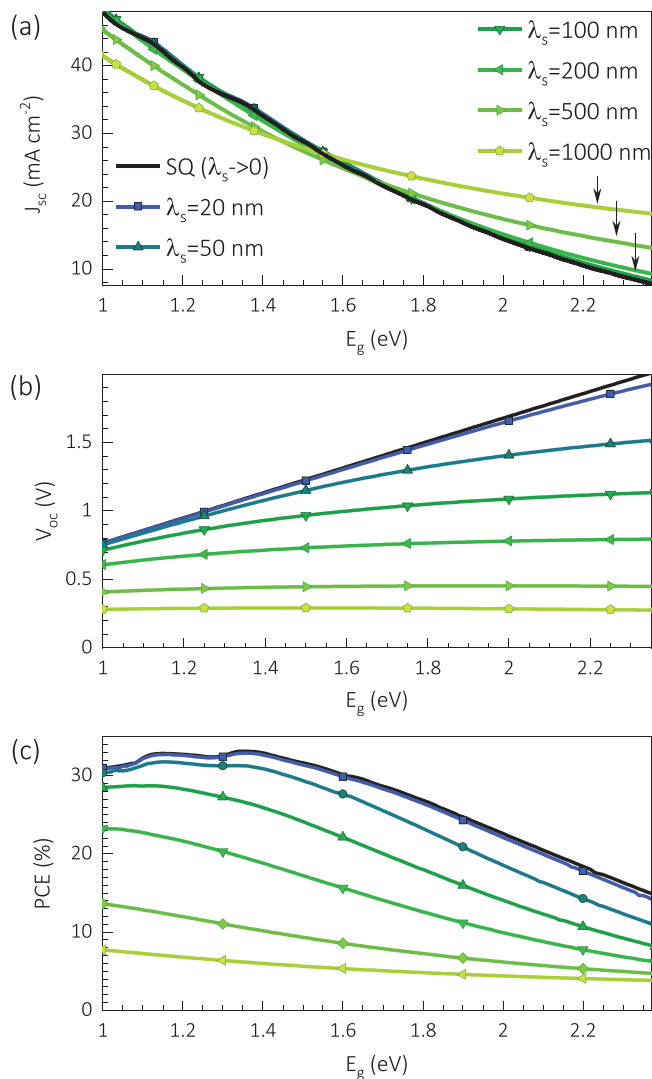


Figure 4. SQ limit of solar cells performance parameters as a function of bandgap energy assuming EQE spectra with different values of the sigmoid wavelength (e.g., see Figure 2b): a) short-circuit current density, b) open-circuit voltage, and c) power conversion efficiency. Emission from both the front and rear contact of the cell was considered.

threshold will lead to an enhancement of J_{sc} that is outbalanced by the simultaneous reduction of V_{oc} . In turn for E_g smaller than the optimum value, adding some EQE below the threshold will enhance the losses associated with both the J_{sc} and the V_{oc} .

For the special case of the sigmoid parameterization of the absorption threshold of the EQE spectrum will always result in values of V_{oc} , FF and PCE below those of the SQ model, independently on how large λ_s can be. However, for EQE spectra whose sigmoid fits reports $\lambda_s > 100$ nm and $E_g > 1.6$ eV, the radiative limit of the photocurrent is not properly described by the step function of the SQ limit at that λ_g value, and a correction should be introduced. In these cases, the appropriate photocurrent theoretical limit can be obtained, from the integral of Equation (2), by using the sigmoid Equation (3) with $A_m = 1$ and depending on both λ_g and λ_s .

3. PV versus Optical Bandgap Energy

From the above analysis, one can correlate the large λ_s values, that is, significantly broad absorption threshold in the EQE spectra, with the presence of i) undesired energy dependent recombination rate and/or ii) poor structural and optoelectronic properties associated with broad density of states, typically parameterized with large E_U . Thus, the use of λ_s as a figure of merit would be advisable: the smaller λ_s the better the device performs. However, care must be taken with the comparison of devices with different bandgaps, for which the corresponding sigmoid energy or energy sloping range is,

$$E_s = E_g \left(\frac{1}{1 - \frac{\lambda_s}{2\lambda_g}} - \frac{1}{1 + \frac{\lambda_s}{2\lambda_g}} \right) \quad (10)$$

where each term in the parenthesis represents the corresponding energy in the energy representation for the positions $\lambda_g \pm \lambda_s/2$ in the wavelength representation (see Figure 2a).

The λ_s - E_g dependence of Equation (10) is illustrated in Figure 5a, where the “ E_s -isolines” show λ_s to be most critical at larger E_g values (see also Figure S5a, Supporting Information). Keeping this in mind, Figure 5b displays E_s as a function of the PCE for several PV technologies, as listed in the “Emerging PV reports.”^[14] The general trend indicates that the larger PCE values present the lesser E_s , and thus the lower λ_s for the

corresponding E_g (see Figure S5a, Supporting Information). Similarly, lower V_{oc} values seem to allow larger E_s (see Figure S5b, Supporting Information). Interestingly, larger E_g exhibit larger E_s values (see Figure S5c, Supporting Information). Overall, the most typical E_s values among the sampled best performing devices are within 25–50 meV, which is between once and twice the thermal energy ($k_B T$) at room temperature (see histogram in Figure 5b).

In addition, besides a few exceptions, the optical bandgap energy (e.g., from absorption Tauc plot) is typically equal or lower than the PV bandgap (from the sigmoid definition for the EQE spectrum), as shown in Figure 5c. Furthermore, in close relation with the λ_s behavior, the difference ΔE_g between these two bandgap energies also decreases in Figure 5d as the PCE does. Similarly, lower V_{oc} exhibit larger ΔE_g values and even some proportionality seems to exist with E_s (see Figure 5b,d and Figure S5b,d, Supporting Information). Also note that ΔE_g is mostly within $0-3k_B T$, at room temperature, being $\Delta E_g < k_B T$ the most common case (see histogram in Figure 5d). Particularly, the energy difference of $k_B T$, at room temperature, has previously been found as a basic mismatch between the methods (Tauc plot versus EQE inflection point).^[16] This suggests that only significantly higher ΔE_g values may be associated with actual physical meaning, like the energy dependent recombination rates discussed in the previous section. In addition, the different distributions in the histograms of Figure 5 may also indicate that larger E_s is not necessarily relating to larger ΔE_g .

In general, it seems that the closer the two definitions of bandgap are, the best, and for most of the top optimized

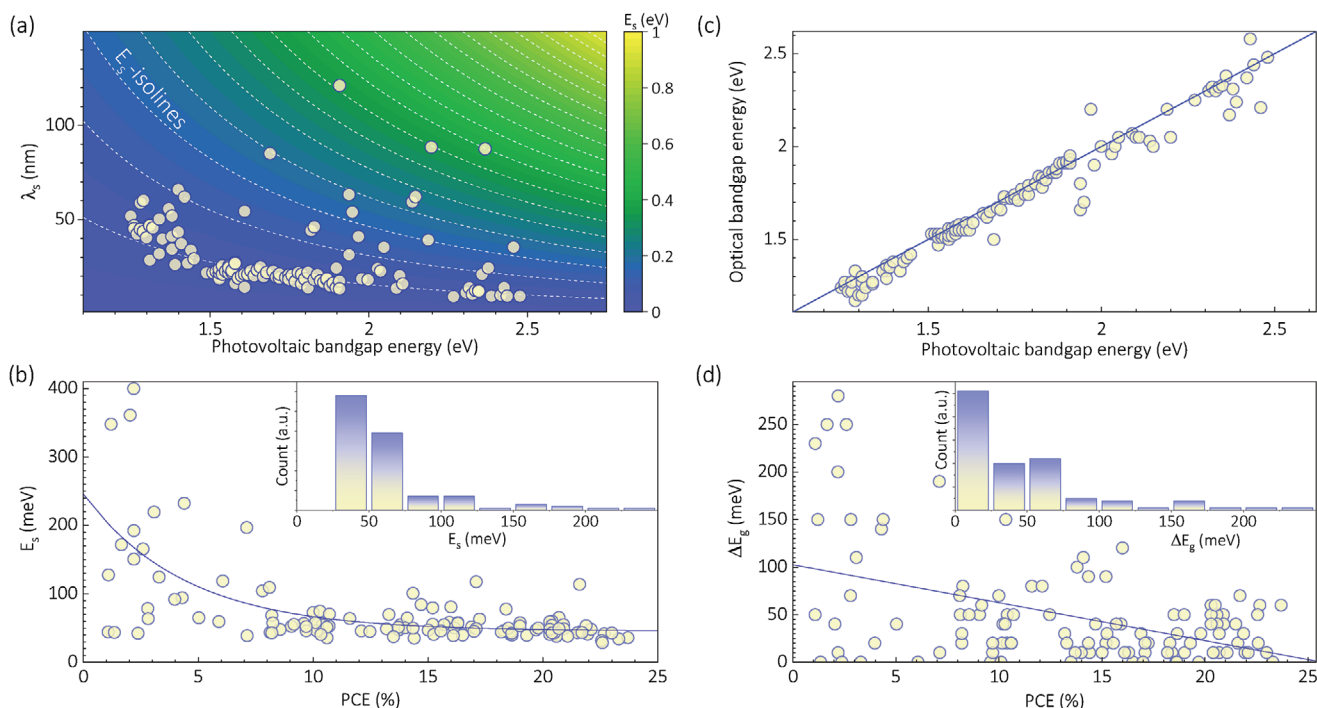


Figure 5. a) Theoretical and b) experimental behavior of the sigmoid wavelength and energy ranges of the EQE spectrum absorption threshold as a function of the bandgap energy and power conversion efficiency, respectively. Difference between photovoltaic and optical bandgap energy, c) one versus the other $E_{g,op}$ ($E_{g,pv}$), and d) absolute mismatch $\Delta E_g = |E_{g,pv} - E_{g,op}|$ as a function of the power conversion efficiency. Insets in (b,d) are the corresponding histograms. The experimental data (circles) is from the “Emerging PV reports.”^[14]

devices $\Delta E_g < k_B T$. The latter means that, for instance, when reporting the photovoltage losses from the optical definition an uncertainty of $\pm k_B T$ would not be critical. However, $\Delta E_g > 3k_B T$ are often found, meaning misvaluations of up to hundreds of mV for the photovoltage losses. In any case, the report of both the optical and PV bandgaps is encouraged.

4. Conclusions

In summary, we have shown that the PV bandgap is effectively determined from the EQE spectrum, as the inflection point at the absorption threshold. However, care must be taken when the EQE spectrum onset shows low sloping, deviating too much from the ideal step-like behavior. By applying a sigmoid function parameterization, we identify two mechanisms (broad λ_g and sub bandgap photocurrent outside $\lambda_g + \lambda_s$) and discuss their physical meaning in terms of Urbach tail and (wavelength dependent) recombination behavior. As a guideline, we propose that the PV bandgap is best determined when the absorption threshold of the EQE spectrum can be properly described by a sigmoid fit with a sloping parameter λ_s smaller than 100 nm. For values $\lambda_s > 100$ nm, the SQ limit value for the photocurrent should be corrected considering both λ_g and λ_s . We also stress on the importance of using the PV bandgap, over the optical bandgap, for reporting limit performance in comparison to the SQ model.

Supporting Information

Supporting Information is available from the Wiley Online Library or from the author.

Acknowledgements

O.A. acknowledges the financial support from the VDI/VD Innovation + Technik GmbH (Project-title: PV-ZUM), the SAOT funded by the German Research Foundation (DFG) in the framework of the German excellence initiative, and the Horizon 2020 project (grant number 871336-PEROXIS). J.G.C. gratefully acknowledges the financial support of the Deutscher Akademischer Austauschdienst (DAAD) through a doctoral scholarship. C.J.B. acknowledges funding from DFG within INST 90/917-1 FUGG, the SFB 953 (DFG, project no. 182849149) and the IKG 2495 (Energy Conversion Systems—from Materials to Devices). C.J.B. further acknowledges the grants “ELF-PV – Design and development of solution processed functional materials for the next generations of PV technologies” (No. 44–6521a/20/4) and “Solar Factory of the Future” (FKZ 20.2-3410.5-4-5) and the SolTech Initiative by the Bavarian State Government.

Open access funding enabled and organized by Projekt DEAL.

Conflict of Interest

The authors declare no conflict of interest.

Data Availability Statement

Research data are not shared.

Keywords

bandgap energy, emerging photovoltaics, external quantum efficiency, solar cells

Received: January 4, 2021

Revised: February 11, 2021

Published online: March 6, 2021

- [1] S. Ravishankar, C. Aranda, P. P. Boix, J. A. Anta, J. Bisquert, G. Garcia-Belmonte, *J. Phys. Chem. Lett.* **2018**, *9*, 3099.
- [2] D. J. Wehenkel, K. H. Hendriks, M. M. Wienk, R. A. J. Janssen, *Org. Electron.* **2012**, *13*, 3284.
- [3] W. Shockley, H. J. Queisser, *J. Appl. Phys.* **1961**, *32*, 510.
- [4] S. Rühle, *Sol. Energy* **2016**, *130*, 139.
- [5] J.-F. Guillemoles, T. Kirchartz, D. Cahen, U. Rau, *Nat. Photonics* **2019**, *13*, 501.
- [6] O. Almora, Y. Zhao, X. Du, T. Heumueller, G. J. Matt, G. Garcia-Belmonte, C. J. Brabec, *Nano Energy* **2020**, *75*, 104982.
- [7] O. Almora, D. Miravet, G. J. Matt, G. Garcia-Belmonte, C. J. Brabec, *Appl. Phys. Lett.* **2020**, *116*, 013901.
- [8] M. Saliba, L. Etgar, *ACS Energy Lett.* **2020**, *5*, 2886.
- [9] X.-Z. Guo, Y.-H. Luo, C.-H. Li, D. Qin, D.-M. Li, Q.-B. Meng, *Curr. Appl. Phys.* **2012**, *12*, e54.
- [10] G. Xue, X. Yu, T. Yu, C. Bao, J. Zhang, J. Guan, H. Huang, Z. Tang, Z. Zou, *J. Phys. D: Appl. Phys.* **2012**, *45*, 425104.
- [11] H. J. Snaith, A. Abate, J. M. Ball, G. E. Eperon, T. Leijtens, N. K. Noel, S. D. Stranks, J. T.-W. Wang, K. Wojciechowski, W. Zhang, *J. Phys. Chem. Lett.* **2014**, *5*, 1511.
- [12] L. Contreras, J. Idigoras, A. Todinova, M. Salado, S. Kazim, S. Ahmad, J. A. Anta, *Phys. Chem. Chem. Phys.* **2016**, *18*, 31033.
- [13] R. B. Dunbar, B. C. Duck, T. Moriarty, K. F. Anderson, N. W. Duffy, C. J. Fell, J. Kim, A. Ho-Baillie, D. Vak, T. Duong, Y. Wu, K. Weber, A. Pascoe, Y.-B. Cheng, Q. Lin, P. L. Burn, R. Bhattacharjee, H. Wang, G. J. Wilson, *J. Mater. Chem. A* **2017**, *5*, 22542.
- [14] O. Almora, D. Baran, G. C. Bazan, C. Berger, C. I. Cabrera, K. R. Catchpole, S. Erten-Ela, F. Guo, J. Hauch, A. W. Y. Ho-Baillie, T. J. Jacobsson, R. A. J. Janssen, T. Kirchartz, N. Kopidakis, Y. Li, M. A. Loi, R. R. Lunt, X. Mathew, M. D. McGehee, J. Min, D. B. Mitzi, M. K. Nazeeruddin, J. Nelson, A. F. Nogueira, U. W. Paetzold, N.-G. Park, B. P. Rand, U. Rau, H. J. Snaith, E. Unger, L. Vaillant-Roca, H.-L. Yip, C. J. Brabec, *Adv. Energy Mater.* **2021**, *11*, 2002774.
- [15] U. Rau, B. Blank, T. C. M. Müller, T. Kirchartz, *Phys. Rev. Appl.* **2017**, *7*, 044016.
- [16] L. Krückemeier, U. Rau, M. Stollerfoht, T. Kirchartz, *Adv. Energy Mater.* **2020**, *10*, 1902573.
- [17] R. Carron, C. Andres, E. Avancini, T. Feurer, S. Nishiwaki, S. Pisoni, F. Fu, M. Lingg, Y. E. Romanyuk, S. Buecheler, A. N. Tiwari, *Thin Solid Films* **2019**, *669*, 482.
- [18] J. Tauc, R. Grigorovici, A. Vanou, *Phys. Status Solidi B* **1966**, *15*, 627.
- [19] M. A. Green, A. W. Y. Ho-Baillie, *ACS Energy Lett.* **2019**, *4*, 1639.
- [20] M. A. Green, Y. Jiang, A. M. Soufiani, A. Ho-Baillie, *J. Phys. Chem. Lett.* **2015**, *6*, 4774.
- [21] Y. Zhao, H. Xu, Y. Wang, X. Yang, J. Duan, Q. Tang, *J. Power Sources* **2019**, *440*, 227151.
- [22] P. Cui, D. Wei, J. Ji, H. Huang, E. Jia, S. Dou, T. Wang, W. Wang, M. Li, *Nat. Energy* **2019**, *4*, 150.
- [23] Y.-N. Zhang, B. Li, L. Fu, Y. Zou, Q. Li, L.-W. Yin, *Sol. Energy Mater. Sol. Cells* **2019**, *194*, 168.
- [24] X. Wang, A. Bolag, W. Yun, Y. Du, C. Eerdun, X. Zhang, T. Bao, J. Ning, H. Alata, T. Ojayed, *J. Mol. Struct.* **2020**, *1206*, 127694.

- [25] Y. S. Tingare, N. So'n Vinh, H.-H. Chou, Y.-C. Liu, Y.-S. Long, T.-C. Wu, T.-C. Wei, C.-Y. Yeh, *Adv. Energy Mater.* **2017**, *7*, 1700032.
- [26] Z. Pei, S. Thiyagu, M.-S. Jhong, W.-S. Hsieh, S.-J. Cheng, M.-W. Ho, Y.-H. Chen, J.-C. Liu, C.-M. Yeh, *Sol. Energy Mater. Sol. Cells* **2011**, *95*, 2431.
- [27] S. Thiyagu, Z. Pei, M.-S. Jhong, *Nanoscale Res. Lett.* **2012**, *7*, 172.
- [28] G. Palma, L. Cozzarini, E. Capria, A. Fraleoni-Morgera, *Rev. Sci. Instrum.* **2015**, *86*, 013112.
- [29] F. Jiang, D. Yang, Y. Jiang, T. Liu, X. Zhao, Y. Ming, B. Luo, F. Qin, J. Fan, H. Han, L. Zhang, Y. Zhou, *J. Am. Chem. Soc.* **2018**, *140*, 1019.
- [30] F. Umar, J. Zhang, Z. Jin, I. Muhammad, X. Yang, H. Deng, K. Jahangeer, Q. Hu, H. Song, J. Tang, *Adv. Opt. Mater.* **2019**, *7*, 1801368.
- [31] X.-Y. Yu, B.-X. Lei, D.-B. Kuang, C.-Y. Su, *Chem. Sci.* **2011**, *2*, 1396.
- [32] L. Wang, D.-B. Li, K. Li, C. Chen, H.-X. Deng, L. Gao, Y. Zhao, F. Jiang, L. Li, F. Huang, Y. He, H. Song, G. Niu, J. Tang, *Nat. Energy* **2017**, *2*, 17046.
- [33] O. Almora, P. Lopez-Varo, K. T. Cho, S. Aghazada, W. Meng, Y. Hou, C. Echeverría-Arrondo, I. Zimmermann, G. J. Matt, J. A. Jiménez-Tejada, C. J. Brabec, M. K. Nazeeruddin, G. Garcia-Belmonte, *Sol. Energy Mater. Sol. Cells* **2019**, *195*, 291.
- [34] B. D. Vezbicke, S. Patel, B. E. Davis, D. P. Birnie Iii, *Phys. Status Solidi B* **2015**, *252*, 1700.
- [35] S. Hood, N. Zarrabi, P. Meredith, I. Kassal, A. Armin, *J. Phys. Chem. Lett.* **2019**, *10*, 3863.
- [36] U. Rau, J. H. Werner, *Appl. Phys. Lett.* **2004**, *84*, 3735.
- [37] S. Zeiske, C. Kaiser, P. Meredith, A. Armin, *ACS Photonics* **2020**, *7*, 256.
- [38] M. A. Green, E. D. Dunlop, J. Hohl-Ebinger, M. Yoshita, N. Kopidakis, A. W. Y. Ho-Baillie, *Prog. Photovoltaics* **2020**, *28*, 3.
- [39] I. Bernalde, E. Medina, M. Rodríguez, S. M. Wasim, G. Marín, C. Rincón, A. Rincón, C. Torres, *Phys. Rev. B* **2004**, *69*, 195201.
- [40] M. Ledinsky, T. Schönfeldová, J. Holovský, E. Aydin, Z. Hájková, L. Landová, N. Neyková, A. Fejfar, S. De Wolf, *J. Phys. Chem. Lett.* **2019**, *10*, 1368.
- [41] S. De Wolf, J. Holovsky, S.-J. Moon, P. Löper, B. Niesen, M. Ledinsky, F.-J. Haug, J.-H. Yum, C. Ballif, *J. Phys. Chem. Lett.* **2014**, *5*, 1035.
- [42] J. Chantana, Y. Kawano, T. Nishimura, A. Mavlonov, T. Minemoto, *Sol. Energy Mater. Sol. Cells* **2020**, *210*, 110502.
- [43] J. Chantana, Y. Kawano, T. Nishimura, T. Minemoto, *Mater. Today Commun.* **2019**, *21*, 100652.
- [44] J. Chantana, T. Nishimura, Y. Kawano, S. Teraji, T. Watanabe, T. Minemoto, *ACS Appl. Energy Mater.* **2019**, *2*, 7843.
- [45] K. Vandewal, S. Mertens, J. Benduhn, Q. Liu, *J. Phys. Chem. Lett.* **2020**, *11*, 129.
- [46] T. Gokmen, O. Gunawan, T. K. Todorov, D. B. Mitzi, *Appl. Phys. Lett.* **2013**, *103*, 103506.
- [47] A. Armin, I. Kassal, P. E. Shaw, M. Hamsch, M. Stollerfoht, D. M. Lyons, J. Li, Z. Shi, P. L. Burn, P. Meredith, *J. Am. Chem. Soc.* **2014**, *136*, 11465.
- [48] L. H. Slooff, S. C. Veenstra, J. M. Kroon, D. J. D. Moet, J. Sweelssen, M. M. Koetse, *Appl. Phys. Lett.* **2007**, *90*, 143506.
- [49] W. J. Yang, Z. Q. Ma, X. Tang, C. B. Feng, W. G. Zhao, P. P. Shi, *Sol. Energy* **2008**, *82*, 106.
- [50] K. Xiong, S. Lu, T. Zhou, D. Jiang, R. Wang, K. Qiu, J. Dong, H. Yang, *Sol. Energy* **2010**, *84*, 1888.
- [51] R. Brendel, M. Hirsch, M. Stemmer, U. Rau, J. H. Werner, *Appl. Phys. Lett.* **1995**, *66*, 1261.
- [52] C. Schinke, D. Hinken, J. Schmidt, K. Bothe, R. Brendel, *IEEE J. Photovoltaics* **2013**, *3*, 1038.
- [53] K. Chi Kao, in *Dielectric Phenomena in Solids with Emphasis on Physical Concepts of Electronic Processes*, Academic Press, Amsterdam **2004**, p. 381.
- [54] A. Melianas, F. Etzold, T. J. Savenije, F. Laquai, O. Inganäs, M. Kemerink, *Nat. Commun.* **2015**, *6*, 8778.
- [55] A. Armin, N. Zarrabi, O. J. Sandberg, C. Kaiser, S. Zeiske, W. Li, P. Meredith, *Adv. Energy Mater.* **2020**, *10*, 2001828.
- [56] U. Rau, *Phys. Rev. B* **2007**, *76*, 085303.
- [57] G. L. Araújo, A. Martí, *Sol. Energy Mater. Sol. Cells* **1994**, *33*, 213.